3. The conditioning chamber was a typical Skinner box, with the floor composed of stainless steel rods through which foot shocks were delivered. The chamber, which was placed in a well-lit room, was wiped with 5% ammonium hydroxide solution before training. Ventilation fans and shock scramblers supplied background noise (78 dB, A-scale). The new chamber, in which tone was tested, was placed in a dark room (with a dim red illumination). The chamber was triangular in shape with an uneven floor. There was no background noise, and the chamber was cleaned with 1% acetic acid.
4. Lesions were produced by passing anodal constant current (1 mA, 10 s) through a stainless steel pin that was insulated with epoxy except for 0.5 mm at the tip. (Stereotaxic coordinates for the hippocampus were as follows: 2.8 mm posterior to bregma, 2.0 mm lateral to midline, and 4.0 mm ventral from the skull surface; 4.2 mm posterior to bregma, 3.0 mm lateral to midline, and 4.0 mm ventral from the skull.)
5. Freezing behavior was assessed by a time-sampling procedure. An observer who was blind to experimental conditions scored each rat every 8 s; R. J. Blanchard and D. C. Blanchard, *Physiol. Psychol.* **67**, 370 (1969); M. S. Fanselow, *Learn. Motiv.* **17**, 16 (1986).
6. R. G. Phillips and J. E. LeDoux, *Behav. Neurosci.* **106**, 274 (1992).
7. L. R. Squire, *Science* **232**, 1612 (1986).
8. J. O'Keefe and L. Nadel, *The Hippocampus as a Cognitive Map* (Clarendon, Oxford, 1978); D S. Olton, J. T. Becker, G. E. Handelmann, *Behav. Brain Res.* **2**, 313 (1979); R. G. M. Morris, P. Garrud, J. N. P. Rawlins, J. O'Keefe, *Nature* **297**, 681 (1982).
9. D. C. Blanchard and R. J. Blanchard, *J. Comp. Physiol. Psychol.* **81**, 281 (1972); B. S. Kapp, R. C. Frysinger, M. Gallagher, J. Haselton, *Physiol. Behav.* **23**, 1109 (1979); J. M. Hitchcock and M. Davis, *Behav. Neurosci.* **100**, 11 (1986); J. Iwata, J. E. LeDoux, D. J. Reis, *Brain Res.* **368**, 161 (1986).
10. R. Bandler, P. Carrive, S. P. Zhang, *Prog. Brain Res.* **87**, 269 (1991); M. S. Fanselow, in *The Midbrain Periaqueductal Gray Matter*, A. Depaulis and R. Bandler, Eds. (Plenum, New York, 1991), pp. 151–173.
11. We thank K. C. Chin for assistance. Supported by an NSF grant (BNS-9008820) to M.S.F.

17 December 1991; accepted 11 March 1992

Microdomains of High Calcium Concentration in a Presynaptic Terminal

R. Llinás,* M. Sugimori, R. B. Silver

Increases in intracellular calcium concentration are required for the release of neurotransmitter from presynaptic terminals in all neurons. However, the mechanism by which calcium exerts its effect is not known. A low-sensitivity calcium-dependent photoprotein (*n*-aequorin-J) was injected into the presynaptic terminal of the giant squid synapse to selectively detect high calcium concentration microdomains. During transmitter release, light emission occurred at specific points or quantum emission domains that remained in the same place during protracted stimulation. Intracellular calcium concentration microdomains on the order of 200 to 300 micromolar occur against the cytoplasmic surface of the plasmalemma during transmitter secretion, supporting the view that the synaptic vesicular fusion responsible for transmitter release is triggered by the activation of a low-affinity calcium-binding site at the active zone.

The role of intracellular free calcium as a trigger for initiating presynaptic transmitter release in chemical synapses was proposed as the "calcium hypothesis" several decades ago (*1*). The mechanism for this Ca^{2+}-dependent transmitter release remains unresolved, partly because the concentration of Ca^{2+} and the distribution of Ca^{2+} concentration within presynaptic terminals during transmission are unknown.

Presynaptic voltage-clamp studies in the giant squid synapse demonstrated a very short (200 μs) latency between Ca^{2+} entry and postsynaptic response, suggesting that Ca^{2+} channels are located at the site of vesicle accumulation and neurotransmitter release (*2*). Moreover, direct measurement of presynaptic Ca^{2+} currents suggested that intracellular free Ca^{2+} concentrations ($[Ca^{2+}]_i$) near the Ca^{2+} channels could be on the order of several hundred micromolar (*3*). Computer models based on these data suggested that the $[Ca^{2+}]_i$ falls off steeply away from the cytoplasmic mouth of the Ca^{2+} channels (*4–7*). These small domes of increased $[Ca^{2+}]_i$ are called microdomains. Each Ca^{2+} channel opening is thought to produce a rapid (microseconds) increase in $[Ca^{2+}]_i$, which rapidly returns to its pre-opening value when the channel closes (*6*). Neurotransmitter release would thus be triggered by a large transient increase in $[Ca^{2+}]_i$ adjacent to the synaptic vesicles.

We have now tested directly the existence of such $[Ca^{2+}]_i$ microdomains by using aequorin (a protein that emits light in the presence of free Ca^{2+}) (*8, 9*) injected in the presynaptic terminal of the giant squid synapse (*10*). In the presence of aequorin, transient increases in $[Ca^{2+}]_i$ appear as flashes of light localized in time and space.

We designed special methodology to identify, image, and characterize these flashes of light. Fluorescent *n*-aequorin-J (minimum Ca^{2+} sensitivity of 10^{-4} M) was injected into the presynaptic terminal (Fig. 1A) (*11*), and its distribution in the terminal was continually monitored by epifluorescence microscopy (*12*). Once the terminal was fully loaded with *n*-aequorin-J (Fig. 1B), the presynaptic fiber was continuously stimulated at 10 Hz (*13*), and a well-defined, stable set of quantum emission domains (QEDs) appeared as white spots (Fig. 1C) (*14*). The superposition of the fluorescent images of the terminal digit (Fig. 1B) and the QEDs (Fig. 1C) revealed that the distribution of QEDs coincided with the presynaptic terminal (Fig. 1D). QEDs were particularly evident at the center of the digit, where most synaptic contacts occur.

We also determined the distribution and number of QEDs in an unstimulated presynaptic terminal at high magnification (Fig. 1F). When QEDs were integrated for 30 s during tetanic stimulation (Fig. 1G), they were found to be organized in regions resembling semicircles or line segments and were approximately equally spaced over the presynaptic digit (Fig. 1, C and G).

Each QED fell within a contiguous rectilinear juxtaposition of approximately 16 pixels (0.25 μm by 0.25 μm per pixel). The size distribution of the QEDs was determined after measuring more than 15,000 such events for both long-term image integrations (1,500 to 5,000 video frames); serially repeated shorter integrations [600 to 1,200 national television standard code (NTSC) video frames]; and sets of single video frames. QEDs fluctuated in size from 0.25 to 0.6 μm^2 (Fig. 2), with a mean of 0.313 μm^2 (range, ~0.25 μm^2 to ~0.375 μm^2). QED patterns such as those shown in Figs. 1 and 2 (areas 0.375 to 0.625 μm^2) represent individual QEDs occurring at nearly identical frame locations, with a small overlap. On average, these sites occupied 8.4% of the presynaptic-postsynaptic membrane contact area, which is close to the 5 to 10% determined by ultrastructural studies (*15*). The number of QEDs in a 70 μm by 40 μm contact area (*15*) was about 4500 (based on actual counting of QEDs in the contact area), quite close to the 4400 calculated for the number of active zones (range 3580 to 5400) from measurements and analysis of transmission electron micrographs (*16*).

The $[Ca^{2+}]_i$ reached during presynaptic activation (200 to 300 μM) was determined by sampling the number of QEDs over consecutive 10-, 15-, or 30-s periods. Many loci repeated periods of photon emission within consecutive sampling periods, as

R. Llinás and M. Sugimori, Department of Physiology and Biophysics, New York University Medical Center, 550 First Avenue, New York, NY 10016, and the Marine Biological Laboratory, Woods Hole, MA 02543. R. B. Silver, Section and Department of Physiology, Cornell University, Ithaca, NY 14853–6401, and the Marine Biological Laboratory, Woods Hole, MA 02543.

*To whom correspondence should be addressed, at the Department of Physiology and Biophysics.

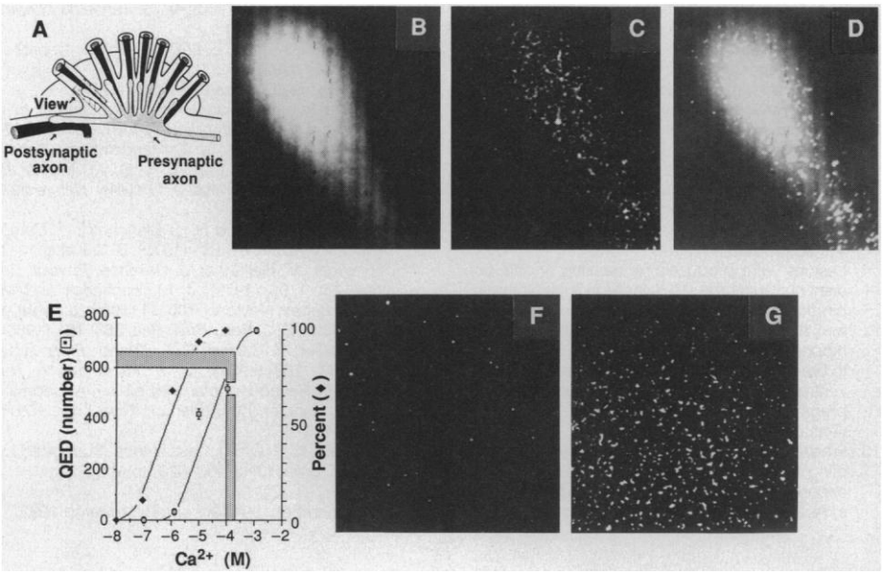

Fig. 1. (**A**) Diagram of the giant squid synapse showing the spatial organization of the presynaptic and the postsynaptic elements. The square (arrow) denotes the location of the synaptic junction shown in (B). (**B**) Fluorescence image of a presynaptic digit injected with a fluorescent preparation of *n*-aequorin-J. (**C**) Video image of photons emitted from QEDs. Image represents the accumulated light emission from *n*-aequorin-J elicited by Ca^{2+} entry during tetanic stimulation (10 s, 10 Hz). (**D**) Superposition of the images in (B) and (C). (**E**) The number of light emissions generated by *e*-aequorin (◆) and *n*-aequorin-J (□) (600 to 650 over a period of 3 s) corresponds to a $[Ca^{2+}]_i$ near 10^{-4} M, about two orders of magnitude less sensitive than the *e*-aequorin response (stippled bar) (*8*, *9*). (**F**) QEDs in an unstimulated terminal (30 s, 10 mM extracellular Ca^{2+}). (**G**) QEDs in the same terminal as in (F) during tetanic stimulation (10 s, 10 Hz).

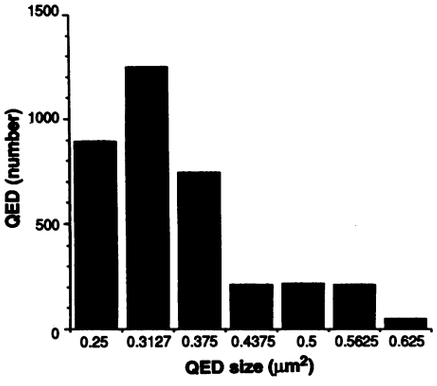

Fig. 2. Distribution of QED size (n = 2500).

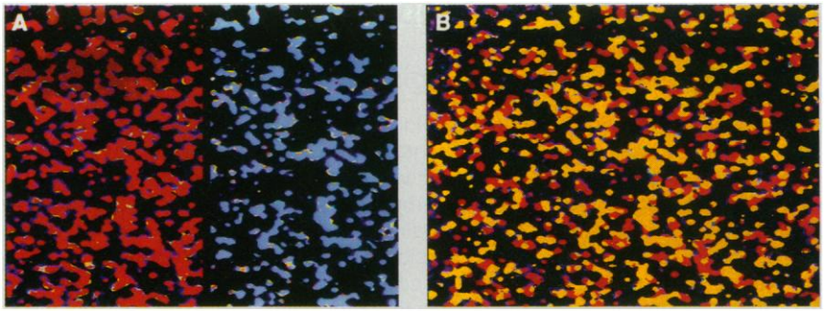

Fig. 3. (**A**) The center portion of two QED images obtained during consecutive 15-s recording intervals from the same area of terminal; the left panel (red) shows the first interval after stimulation; the right panel (blue) shows the subsequent 15-s period (blue). (**B**) The superposition (>93%) of the QEDs from consecutive 15-s recording intervals in (A) (red and blue) appears yellow.

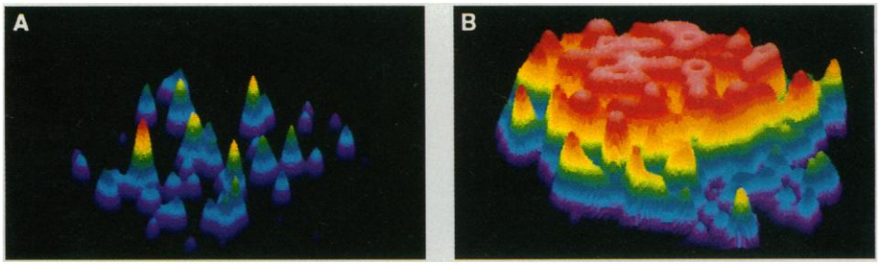

Fig. 4. Three-dimensional projection after image integration (4800 frames, 30-Hz sampling rate) of the QED image in a terminal bulb of a presynaptic fiber (**A**) before stimulation and (**B**) during stimulation, illustrating the steepness of the Ca^{2+} microdomain profiles. Image intensities were segmented into an 8-bit range, with the maximum intensity corresponding to the video intensity level of 255 (white) and the lowest to a level of 0 (black), with intermediate levels ranging from high (red) through intermediate (yellow and green) to low (blue) probabilities that a particular microdomain would be active.

shown in Fig. 3, A and B, for two consecutive 15-s periods, indicating that Ca^{2+} entry tended to be organized temporally and spatially. QEDs detected during the first 15-s period (Fig. 3A, red) and those detected during the second 15-s period (Fig. 3A, blue) are shown as yellow spots in Fig. 3B. When the second period is compared to the first period, there is an area correspondence of ~95%; when the order for comparison was reversed, the correspondence was 87%. Subsequent sequential 15-s periods, having correspondences between 93 and 98.81%, indicate that within such time most of the sites of Ca^{2+} entry to the terminal are activated.

Prolonged integrations (1200 to 5000 video frames) were performed during stimulation to determine the percentage of the total presynaptic terminal area containing QEDs. Figure 4 corresponds to the terminal bulb of a presynaptic fiber before (Fig. 4A) and during (Fig. 4B) stimulation (as in Fig. 1A). The average clearly describes areas of high probability of light emission and the pronounced differences between the prestimulation and stimulatory conditions. Because of the long integration times used, fused rather than discrete QEDs were observed in both cases. The distribution of $[Ca^{2+}]_i$ was not random and often formed ringlike structures, lines, or combinations of these. These patterns probably correspond to the "fingerprints" of clawlike postsynaptic dendrites that contact the presynaptic digit in the active zone (*17*).

Detailed analysis of the temporal and spatial distribution of QEDs suggests that once a microdomain is activated, the tem-

poral repeat frequencies at which a particular microdomain is activated differ from those of the same microdomain before stimulation. Upon activation, three classes of temporal repeat frequencies, not seen under prestimulation conditions, appeared, the primary temporal class having a mean delay period between the initial activation and subsequent activation of 1.37 s, which may indicate temporal requirements or constraints upon reestablishing microdomain activation. Under stimulation, the lifetime of a QED averaged 200 ms, clearly a high value that is likely attributable to the photon efficiency and lag characteristics of the camera and light-intensity losses through the optical system. Under most conditions, QEDs that occurred as singlets or doublets did not occur at high frequency at any particular microdomain. Analysis of the activation dynamics of individual microdomains suggested a quasi-sequential activation, that is, a low probability of immediate reactivation. One possible mechanism for this refractory period may be related to the high $[Ca^{2+}]_i$ at the active zone or to the low number of readily releasible vesicles. In fact, high $[Ca^{2+}]_i$ depresses Ca^{2+} channel activity by blocking the channel and increasing its inactivation (*18*). Also, it is well documented that an average of one vesicle is normally released per active zone (*15, 19, 20*). In fact, in squid, the quantum content is 5000, close to the value of 4500 measured here; thus, there must be an average of one vesicle per active zone. The presence of such "lateral inhibition," by activation of a certain number of channels in an active zone patch (average measured area, 0.313 μm^2), would temporarily depress local channel activity. If this were so, a special kinetics would operate, in which the probability of release is related to the previous activity in any given active zone (*21*). This prospect adds an interesting new variable to incorporate into models of transmitter release.

The distribution of Ca^{2+} microdomains suggests that these sites are active zones where increased $[Ca^{2+}]_i$ triggers neurotransmitter release by binding to a low-affinity Ca^{2+}-binding site at the presynaptic vesicles and activating the release process. Such a mechanism would safeguard the synapse from large amounts of spontaneous transmitter release because probably more than one Ca^{2+} channel must be activated per active zone to trigger exocytosis (*6*). Also, there would be enough time to replace the expended vesicles (*6*). The short delay between Ca^{2+} entry and transmitter release suggests that only vesicles near the QEDs would be released by a given action potential (*2*). The fact that $[Ca^{2+}]_i$ attains such high concentrations at release sites must be taken into account in the study of the mechanisms of membrane fusion.

REFERENCES AND NOTES

1. B. Katz, *The Release of Neurotransmitter Substances: The Sherrington Lectures X* (Thomas, Springfield, IL, 1969).
2. R. Llinás, in *Approaches to the Cell Biology of Neurons*, W. M. Cowan and J. A. Ferendelli, Eds. (Society for Neuroscience, Bethesda, MD, 1977), vol. 2, pp. 139–160.
3. _____, I. Z. Steinberg, K. Walton, *Biophys. J.* **33**, 323 (1981).
4. J. E. Chad and R. Eckert, *ibid.* **45**, 993 (1984).
5. S. M. Simon, M. Sugimori, R. Llinás, *ibid.*, p. 264a.
6. S. M. Simon and R. Llinás, *ibid.* **48**, 485 (1985).
7. R. S. Zucker and A. L. Fogelson, *Proc. Natl. Acad. Sci. U.S.A.* **83**, 3032 (1986).
8. O. Shimomura, B. Musicki, V. Kishi, *Biochem. J.* **261**, 913 (1989).
9. O. Shimomura, S. Inouye, B. Musicki, Y. Kishi, *ibid.* **270**, 309 (1990).
10. A preliminary note on these results has appeared [R. Llinás, M. Sugimori, R. B. Silver, *Biol. Bull.* **181**, 316 (1991)].
11. The compound *n*-aequorin-J, a chemically modified low-sensitivity form of a naturally occurring photoprotein (*8*), was pressure-injected (tip concentration 5%) [R. Llinás, J. R Blinks, C. Nicholson, *Science* **176**, 1127 (1972)] into the presynaptic terminal. To aid in localization of aequorin within the preparation, 5% of the aequorin injected was also fluoresceinated.
12. Video images were obtained with the use of a direct optical extension onto a dual-microchannel plate-intensified Video-Intensified Microscopy (VIM) camera system (Hamamatsu Argus 100; Hamamatsu Photonics, Inc., Bridgewater, NJ), operated in photon-counting mode, or a Nikon Optiphot-pol microscope modified to simultaneously record multispectral luminescent specimens (R. B. Silver, unpublished data); that is, we obtained differential interference contrast (DIC) or fluorescence images (Dage/MTI Model 68 SIT camera) and single-photon aequorin images (Hamamatsu C2400-20 VIM camera, pedestal set to background-shot noise). Video systems were operated at an NTSC frame-sampling rate of 30 Hz. The background signal of the optical system was typically fewer than 60 events per minute (determined for 10^3 or 10^4 s over the entire field); signal-to-noise ratio was ~150:1.
13. Stellate ganglia from small *Loligo pealii* were dissected and synaptic transmission was monitored with standard methods [R. Llinás, I. Z. Steinberg, K. Walton, *Biophys. J.* **33**, 289 (1981)]. Results were obtained from 27 synapses bathed in artificial seawater (10 mM Ca^{2+}).
14. Video images were processed, filtered, and analyzed to assist in QED feature extraction and quantification with a Hamamatsu Argus 100 imaging system or an Imagel-AT (Universal Imaging Corp., West Chester, PA) running on a Dell 325 AT-bus computer. Aequorin luminescence images of QEDs, seen as discrete spots on an otherwise dark background, were analyzed as single-video frames, as integrations of multiple-video frames (range, 10 to 4800), or as digitized sequential frames. Calibration curves were constructed by measuring the number of Ca^{2+}-dependent light flashes (within 33-ms frame-integration periods), each resulting from a discrete interaction of Ca^{2+} with an aequorin molecule (*8, 9*), that accumulated during the 3 s after 20 pl of aequorin was injected into 10^{-3} to 10^{-8} M Ca^{2+} [R. B. Silver, *Dev. Biol.* **131**, 11 (1989)]. Two procedures were followed for accumulating information: (i) light-emission points were accumulated during 3 s of stimulation, and the QED distribution was studied; (ii) two portions of the recording field were individually accumulated and compared.
15. D. W. Pumplin, T. S. Reese, R. Llinás, *Proc. Natl. Acad. Sci. U.S.A.* **78**, 7210 (1981).
16. D. W. Pumplin and T. S. Reese, *Neuroscience* **3**, 685 (1978).
17. J. Z. Young, *Brain Res.* **57**, 457 (1973).
18. G. P. H. Young *et al.*, *Proc. Natl. Acad. Sci. U.S.A.* **81**, 5155 (1984).
19. J. Korn, A. Mallet, A. Triller, D. S. Faber, *J. Neurophysiol.* **48**, 679 (1982).
20. A. Triller and H. Korn, *ibid.*, p. 708.
21. R. Llinás, T. L. McGuinness, C. S. Leonard, M. Sugimori, P. Greengard, *Proc. Natl. Acad. Sci. U.S.A.* **82**, 3035 (1985).

22. We thank O. Shimomura (Marine Biological Laboratory) for the custom aequorin preparations. Supported by the NIH (NS13742 to R.L.), the U.S. Air Force (AFOSR89-0270 to R.L.), the NSF (DGB-9005343 to R.B.S.), and the Cornell–U.S. Army Biotechnology Center of Excellence Program (24629-LS-UIR to R.B.S.).

8 December 1991, accepted 6 March 1992